Towards synergistic combination of biochar/ultrasonic persulfate enhancing removal of natural humic acids from water

Hongbo Liu, Mengting Ye, Zhenxing Ren, Eric Lichtfouse, Zhongbing Chen

Journal of Environmental Chemical Engineering 10 (2022) 107809

https://doi.org/10.1016/j.jece.2022.107809

Towards synergistic combination of biochar/ultrasonic persulfate enhancing removal of natural humic acids from water

Hongbo Liu [a,*], Mengting Ye [a], Zhenxing Ren [a], Eric Lichtfouse [b], Zhongbing Chen [c]

[a] School of Environment and Architecture, University of Shanghai for Science and Technology, 516 Jungong Road, 200093 Shanghai, China
[b] Aix-Marseille Univ, CNRS, IRD, INRA, Coll France, CEREGE, 13100 Aix en Provence, France
[c] Faculty of Environmental Sciences, Czech University of Life Sciences Prague, Kamýcká 129, 16500 Prague, Czech Republic

Keywords:
Humic acids (HAs)
Biochar
Persulfate (PS)
Ultrasonic treatment
Hydroxyl radical

A B S T R A C T

Removal of natural organic matter (NOMs) from actual water is a major challenge in the context of worldwide pollution of natural water resources. The removal of humic acids in a system combining biochar adsorption and ultrasonic persulfate oxidation was studied in this paper. The effects of biochar addition, persulfate concentration and initial pH were investigated. A high removal rate of humic acids up to 92.5% was achieved for the combined biochar/ultrasonic/persulfate system, versus 84.0% for combined biochar/persulfate, 52.0% for sole biochar, 50.0% for combined biochar/ultrasonic, 10.0% for combined persulfate/ultrasonic, 4.0% for sole ultrasonic and 1.0% for sole persulfate systems. Ultrasonic treatment increased the removal efficiency of humic acids to 90.0% within 60 min. Mechanisms towards synergistic combination of the biochar/ultrasonic/persulfate system were investigated by gel permeation chromatography, electron paramagnetic resonance and quenching experiments together with the characterization of biochar. Hydroxyl radical and the adsorption of biochar were the major contributors to the proposed synergistic adsorption-oxidation removal mechanism, followed by the sulfate radical $SO_4^{\cdot-}$. The results of three-dimensional fluorescence diagram, fluorescence regional integration and TOC analysis indicated that the system presented promising application prospects to remove NOM pollutants from real water.

1. Introduction

Advanced oxidation processes (AOP) have been widely used to remove organic contaminants such as 1,4-dioxane, dyes and pharmaceuticals from water [1–4]. In particular, the use of the sulfate radical $SO_4^{\cdot-}$, generated by activation of peroxymonosulfate or persulfate, has been emerged as an alternative to the hydroxyl radical •OH, due to the facts that $SO_4^{\cdot-}$ has a longer half-life of 30–40 μs compared to below 1 μs for •OH, a broader pH range of 3.0–11.0, and a higher redox potential of 2.5–3.1 V versus 1.9–2.7 V for •OH [5,6]. Peroxymonosulfate or persulfate can be activated by heat, UV light, ultrasonic and microwaves, etc. However, the use of persulfate alone has limitations such as high energy consumption, moderate deficiency and secondary pollution[7]. Similarly, the use of biochar alone for pollutant adsorption is limited by biomass sources and pyrolysis temperature. Therefore, recent studies are focusing on development of combined AOP processes removing organic pollutants. For instance, 98.8% of Acid Red 88 was removed by a porous biochar-supported Fe-Mn composite [8]. Combination of microwave, natural magnetite (Fe_3O_4) and persulfate has also achieved 94.2% removal of *p*-nitrophenol within 28 min [9].

Ultrasonic irradiation (US) combined with persulfate is efficient in removing organic pollutants via acoustic cavitation and sono-activated persulfate oxidation. The generation, growth and collapse of cavitation micro-bubbles during sonication induce a local temperature of about 5000 K, and a pressure of about 500 bar [10]. This induces spliting of water into hydoxyl radicals, which can further oxidize organic contaminants. Sonication can also produce $SO_4^{\cdot-}$ in the presence of persulfate. Therefore hybrid processes combining sonication and persulfate have been recently investigated to remove valsartan, bisphenol AF, propranolol and amoxicillin [11–14]. So far, the exact synergistic effects of combined biochar and sonication on natural organic matter (NOM) removal from water have been seldom studied. Here we investigated the removal of humic acids (HAs) as a model pollutant of NOM in water by sonication with biochar and persulfate. We studied the effects of initial humic concentration, persulfate dosage, pH and biochar dosage on performances of the combined process. Active radical species were

* Corresponding author.
E-mail address: Liuhb@usst.edu.cn (H. Liu).

identified by free radical quenching and electron paramagnetic resonance (EPR) investigations; while the practicability of the combined process is verified by experiments with real water from the Yangtze River through fluorescence regional integration (FRI) and total organic carbon (TOC) analysis. Finally, a possible removal pathway of the combined process is proposed.

2. Materials and methods

2.1. Chemicals and reagents

The synthesis and characterization of the biochar were described in our previous study [15]. Chemicals such as 5,5-dimethyl-1-pyrroline N-oxide (DMPO, purity>99.0%) were obtained from Sigma–Aldrich. The real water samples were collected from the Qingcaosha reservoir of the Yangtze River. All reagents were analytically pure and employed without pre-treatments.

2.2. Experimental procedures

Batch removal experiments were conducted in an ultrasonic reactor (53 kHz). According to the perform calorimetry [16], the actual power used in the experiment was 60 W. The real-time temperature in the water was detected by a thermometer. When the temperature increased, additional cold water was introduced into the reactor to maintain a certain temperature. 100 mL of humic solution was added into a 250 mL conical flask for batch experiments. For experiments without ultrasonic application, an incubator was used with the shaking speed at 200 rpm and the experiments were conducted under a constant temperature of 25 ℃. Unless otherwise specified, the reaction conditions were established as follows: $[HAs]_0 = 5$ mg/L, $[persulfate]_0 = 1$ mM, [biochar]= 0.7 g/L, [ultrasonic]= 60 W and pH= 9. For each batch experiment, 5 mL reaction suspension was taken out at the given time intervals and filtered immediately through a 0.45 μm membrane to remove residue biochar. In order to study the impact of each key factor, parameters were varied within certain ranges, namely persulfate dosages (0.4–1.2 mM), biochar dosages (0.1–0.7 g/L), initial concentration of HAs (5–15 mg/L) and pH (5.0–9.0) (Table 1).

2.3. Analytical methods

Changes in concentration of HAs, composition and TOC during the reaction process were measured as described in our previous work [15]. Wavelength scan and gel permeation chromatography (GPC) were used to further investigate the change of molecular weight and the removal of HAs. The identification of active radicals were analyzed by the electron paramagnetic resonance method (EPR, Bruker EMXPLUS).

2.4. Kinetic model, synergy index and removal rate of HAs

The removal rate of HAs was calculated as described in our earlier investigation [15]. The removal kinetics of HAs were analyzed using the following pseudo-first-order kinetic model as described with Eq. (1):

$$\ln(C_t/C_0) = -k_{obs}t \quad (1)$$

where C_0 and C_t represent concentrations of HAs (mg/L) at the initial time and time t, respectively, and k_{obs} represents the reaction rate constant (min^{-1}).

Synergy index was calculated through Eq. (2) to justify the synergism or antagonism of the ultrasonic on persulfate activation.

$$Synergy \quad index = \frac{K_{US/BC-PS}}{K_{US} + K_{BC-PS}} \quad (2)$$

> 1, synergistic effect; < 1, antagonism effect.

Where *synergy index*, $K_{US/BC\text{-}PS}$, K_{US} and $K_{BC\text{-}PS}$ represents the reaction rate constant (min^{-1}) of the biochar/persulfate/ultrasonic, ultrasonic and biochar/persulfate systems respectively.

The spectral coefficient S_R can be calculated by the wavelength scanning spectrum of UV–vis in the range of 200–800 nm to demonstrate the change of the average molecular weight of HAs before and after reaction (Eqs. (3) and (4)).

$$a_\lambda = 2.303 \times UV_\lambda \quad (3)$$

$$S_R = S_{(275-295)} / S_{(350-400)} \quad (4)$$

Where a_λ represents absorption coefficient at the wavelength of λ nm, UV_λ represents the measured absorbance value at the wavelength of λ nm, $S_{(275-295)}$ is the slope of the linear regression equation of $log\ (a_\lambda)$ at wavelength of 275–295 nm, and $S_{(350-400)}$ is the slope of the linear regression equation of $log\ (a_\lambda)$ at wavelength of 350–400 nm.

3. Results and discussion

3.1. Characterization of the biochar prepared

The thermogravimetric analysis (TGA) was applied to explore the thermal stability and composition changes of the biochar prepared (Fig. 1a). At the first stage (0–200 ℃), an apparent loss peak appeared around 81 ℃. Due to the loss of volatile substances and water, the corn stalks lost 12% of their weight. Two weight loss peaks of 324 ℃ and 371 ℃, found at the second stage (200 ℃−400 ℃), with the weight loss of about 59.0% were attributed to the decomposition of unstable hemicellulose, cellulose and some lignin components in the sample. The third stage was the process of sample carbonization and aromatization (400–900 ℃), including the decomposition of organic matter with strong thermal stability. With the increase of temperature, the inorganic impurities contained in biochar were less, which is conducive to improve the performance of the biochar [17].

Roman spectra of the study biochar was demonstrated in Fig. 1b. The two main characteristic peaks at 1340 cm^{-1} and 1601 cm^{-1} corresponded to peaks D and G respectively. Band D is associated with the degree of disorder, while band G is associated with the level of graphitization of materials. The intensity ratio of band D and G (I_D/I_G) represents the degree of defects in biochar, whose value increases with the disordered structure existing in the carbon [18]. Previous studies have reported that the process of pyrolysis could increase the degree of defect on the boundaries of biochar and induce more functional groups [19, 20].

As shown in Fig. 1c, the FTIR spectrum showed peaks at 3437 cm^{-1}

Table 1
A list of experimental parameters.

Experimental variables	Experimental parameters				
	Biochar dosages (mg/L)	Persulfate dosages (mM)	Humic concentration (mg/L)	pH value	Ultrasonic power (W)
Biochar dosages	0.1/0.3/0.5/0.7	1.0	5.0	9.0	60
Persulfate dosages	0.7	0.4/0.8/1.0/1.2	5.0	9.0	60
Humic acids concentration	0.7	1.0	5.0/10.0/15.0	9.0	60
pH value	0.7	1.0	5.0	5.0/6.0/7.0/8.0/9.0	60

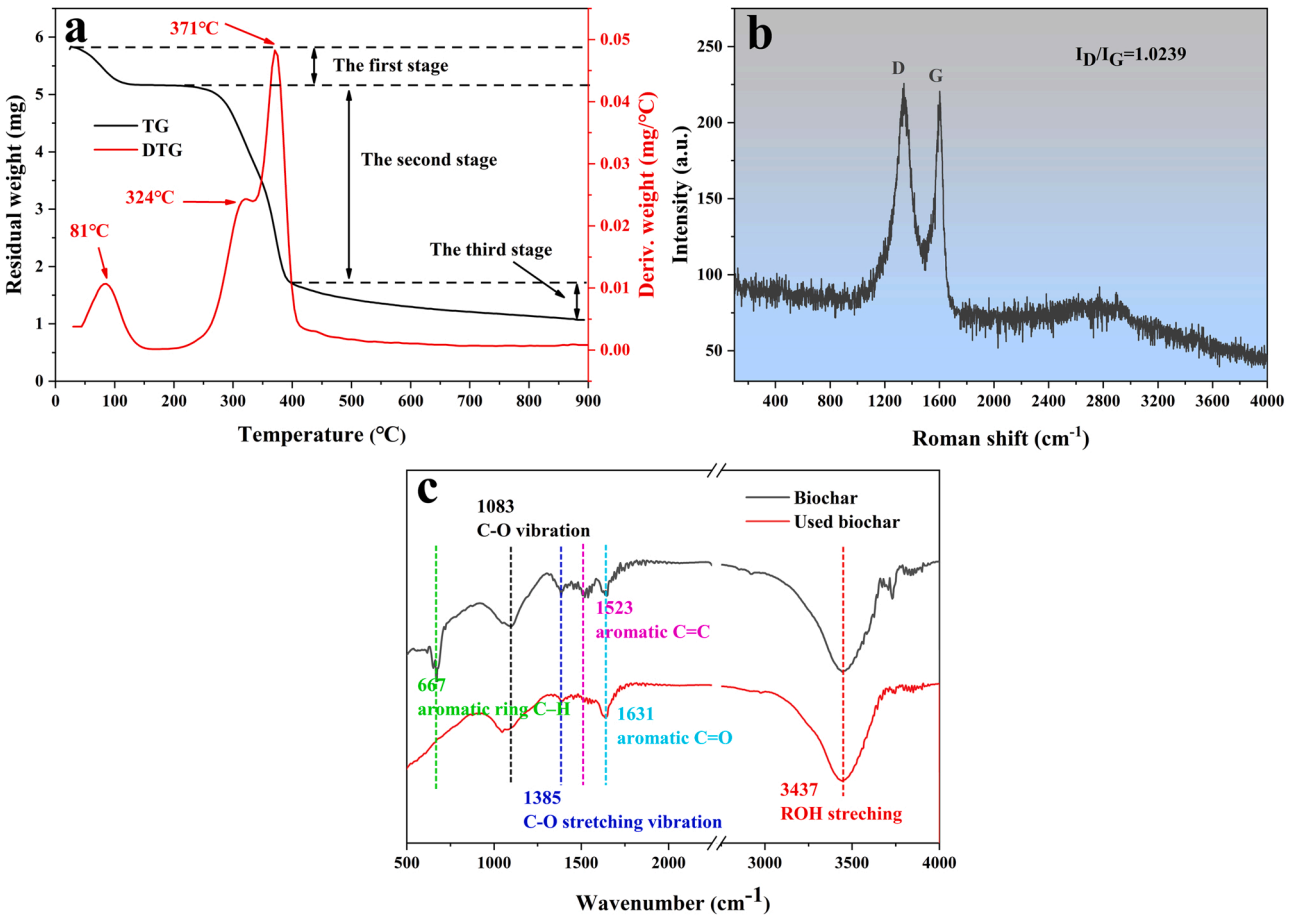

Fig. 1. (a)TG-DTG curves of the biochar precursor; (b) Raman spectra of biochar and (c) FTIR of biochar before and after reaction ([biochar] = 0.7 g/L, $[persulfate]_0$ = 1 mM, [humic acids] = 5 mg/L, pH= 9, [ultrasonic] =60 W).

and 1083 cm^{-1}, which were characteristic peaks of the –OH and C-O groups in carboxyl and phenol respectively [21,22]. The peaks around 1631 cm^{-1},1523 cm^{-1}, 667 cm^{-1} and 1385 cm^{-1} belong to the stretching of C═O, C═C, C–H and C-O, respectively [23,24]. From the FTIR analysis results, various functional groups were found on the original surface and the used biochar, which function as important adsorption and active catalytic sites for the later reaction. Notably, the peak intensity of C-OH decreased with the increase of C═O intensity after reaction. XPS scan of biochar was carried out to verify relative amount of the functional groups.

Fig. 2a and b showed XPS characterization of the original biochar and the used biochar respectively. Two characteristic peaks of C1s and O1s could be observed for biochar at 284.7 eV and 532.7 eV, respectively. After reaction, the oxygen content increased obviously, which might be aroused by oxidation at the surface of biochar. Fig. 2c, d, e and f manifested the specific change of different functional groups. The original peak of C1s could be interpreted as five components of C-graphite/C-C/C-H, C-OH/C-O-C, COOH, C═O and π-π* shake-up at 284.76 eV, 285.8 eV, 288.94 eV, 286.28 eV and 290.03 eV, respectively. For the used biochar, four main compounds centering at 284.84 eV, 288.38 eV, 286 eV and 290.92 eV could also correspond to C-graphite/C-C/C-H, COOH, C═O and π-π* shake-up respectively. The O1s high-resolution scans of biochar was also implemented. The change of O1s was in line with that of C1s. The results of XPS characterization indicated that the content of C═O and C═O-OH increased after reaction. On the contrary, the content of C-graphite/C-C/C-H and C-OH/C-O-C reduced after reaction, implying the transformation of surface functional groups of the biochar, which was consistent with the results of FTIR analysis. In some previous studies, biochar surfaces have also been found to have a lot of oxygen-containing functional groups and, especially, C–C and –C–O groups could be oxidized to –C═O when biochar and persulfate coexisted [25,26]. Based on the above investigations and results of other studies, we speculate that the C-OH group might act as active sites for persulfate activation.

3.2. Synergistic removal of HAs by sole and combined ultrasonic-enhanced biochar/persulfate systems

To better understand the role of ultrasonic treatment in the combined process, the following reaction processes were investigated: ultrasonic treatment, persulfate treatment, biochar treatment, combined persulfate/ultrasonic treatment, combined persulfate/biochar treatment, combined biochar/ultrasonic treatment and biochar/persulfate/ultrasonic treatment (Fig. 3a). It was found that almost no depletion of HAs was obtained when persulfate was applied to the solution alone. A slight reduction of humic acids was observed for the individual ultrasonic treatment (4.0%). A removal efficiency of 10.0% in HAs could be obtained with the combined persulfate/ultrasonic treatment system. The researchers summarized the reason for this phenomenon as that cavitation, extreme environment of high temperature and high pressure produced by ultrasonic broke the O-O bond in persulfate, which made persulfate better activated, contributing to more free radicals participating in the reaction and improving the removal effect of the substrate [27,28]. A similar removal effect was also observed in the biochar/ultrasonic treatment system. The removal of HAs increased from 52.0% to 84.0% after 120 min reaction with the combination of biochar and persulfate, indicating that biochar and persulfate presented synergistic effects. Interestingly, the removal of HAs increased from 52.0% to

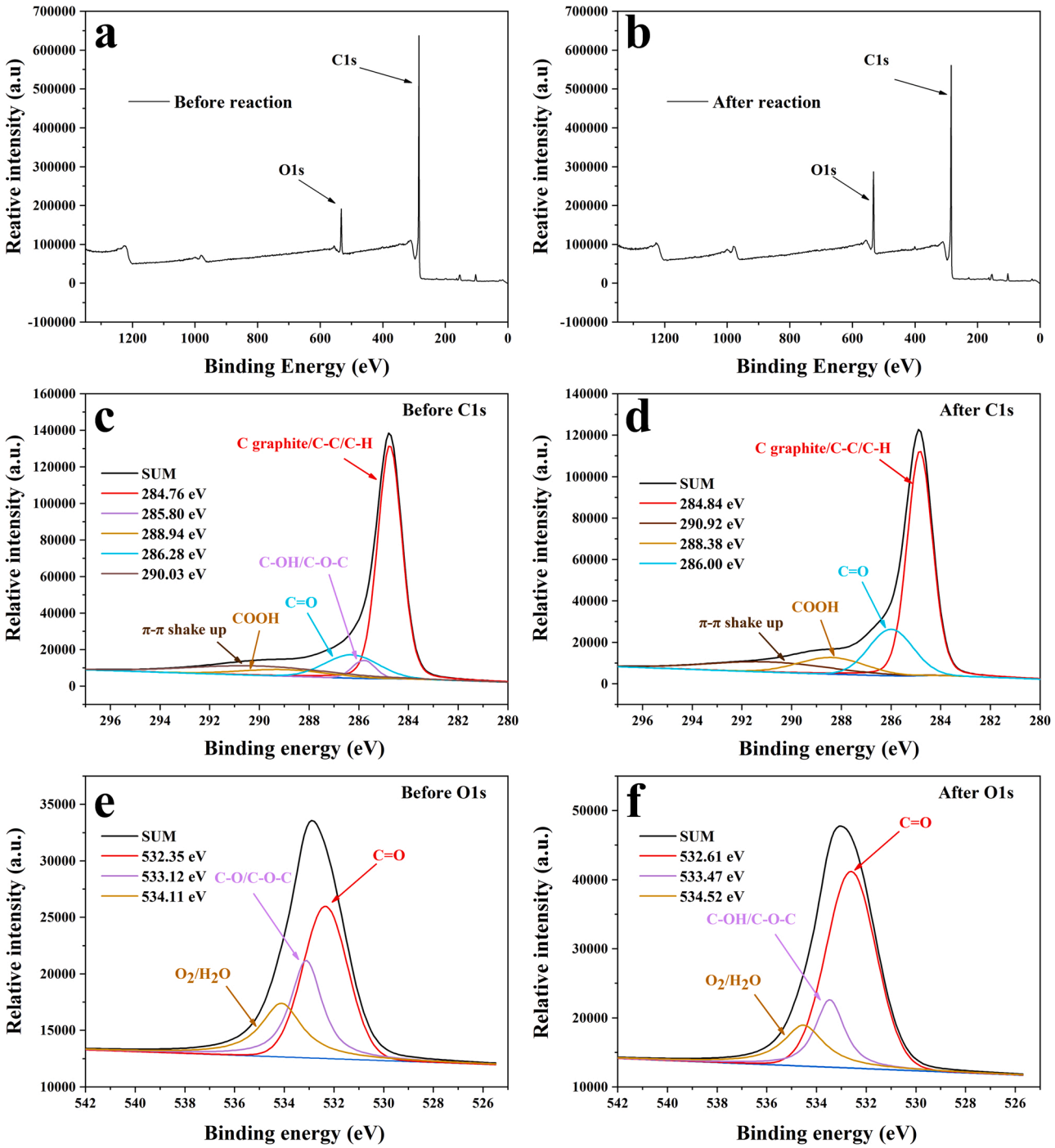

Fig. 2. XPS survey of biochar before (a) and after reaction (b);(c) C1s and (d) O1s high-resolution scans of biochar before reaction;(e) C1s and (f) O1s high-resolution scans of biochar after reaction.

90.0% after 60 min of ultrasonic treatment to the biochar/persulfate system. In generation, persulfate decomposition caused a large amount of H^+ to be released in the water and the generation of HSO_4^- [29]. Many studies have reported that the pH value during persulfate reaction is much lower [30]. It could be seen from Table S1 that the pH changes of the other systems were small except that the final pH in the biochar/ persulfate and biochar/ persulfate / ultrasonic systems dropped to about 3.0. It could be reasonably inferred that, except for the biochar/ persulfate and biochar/ persulfate / ultrasonic systems, other systems have weak ability to activate persulfate, and the decomposition of persulfate was insignificant.

The data in Fig. 3b demonstrated pseudo-first-order kinetics for removal of HAs, with the corresponding k_{obs} constants for ultrasonic treatment, persulfate, combined persulfate/ultrasonic, combined biochar/persulfate, combined biochar/ultrasonic and combined biochar/ persulfate /ultrasonic treatments of 2.60×10^{-4}, 5.05×10^{-5}, 8.79×10^{-4}, 1.2×10^{-2}, 3.51×10^{-3} and 3.4×10^{-2} min^{-1}, respectively. Ultrasonic treatment improved the reaction rate and shortened the reaction time of the system. The synergistic index was calculated as 2.76, which further proved the synergism between ultrasonic treatment and biochar/persulfate.

Fig.3c showed the adsorption wavelength scan before and after 120 min of reaction for the biochar/persulfate/ultrasonic system. The absorption peaks at 254 nm and 400 nm were attributed to benzene

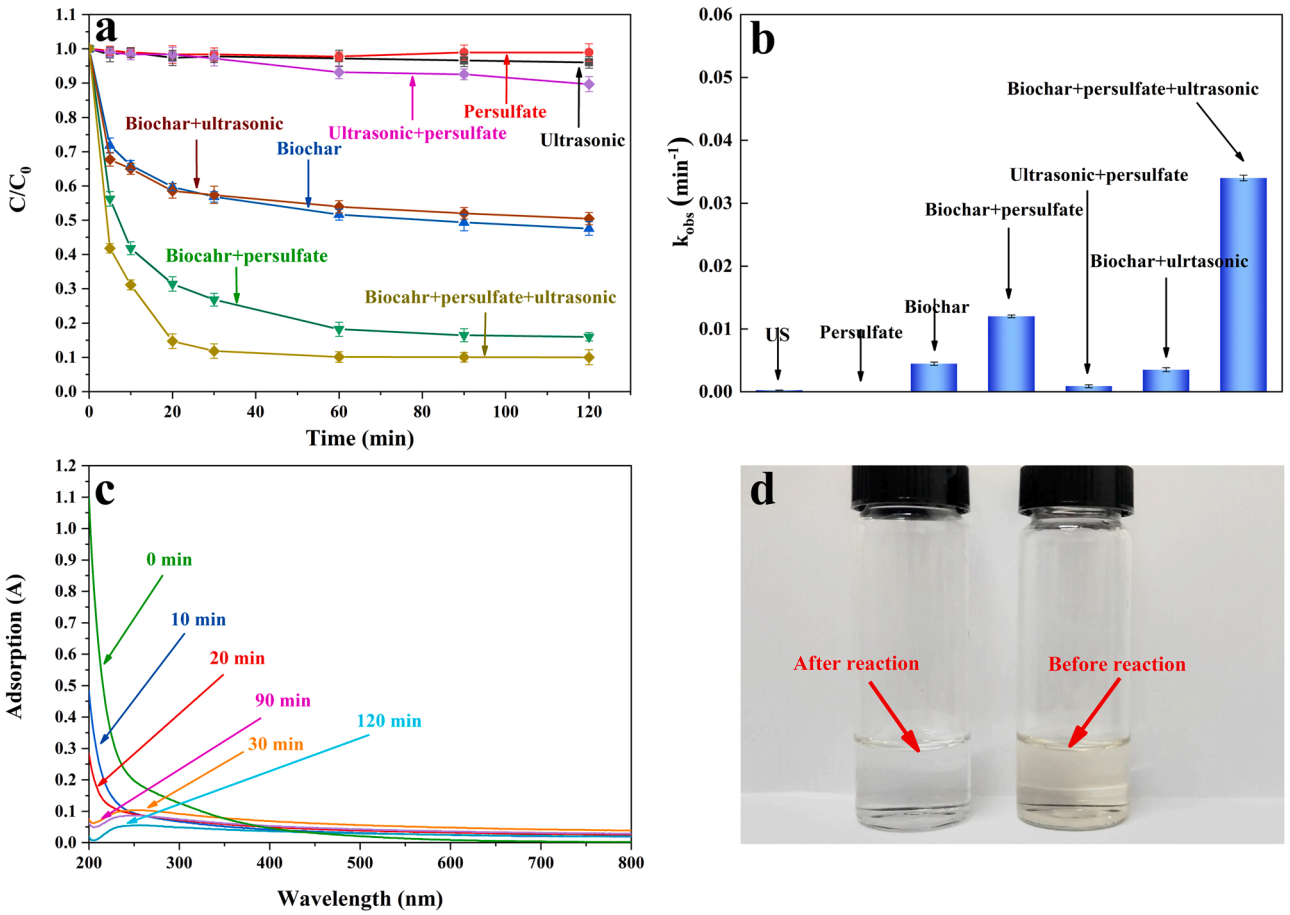

Fig. 3. (a) Removal of humic acids; (b) k_{obs} of humic acids under different reaction system. (c) UV–vis of 5 mg/L HA before and after reaction and (d) the color change of the solution before and after the reaction. Reaction conditions: [humic acids] = 5 mg/L, $[persulfate]_0$ = 1 mM, [biochar] = 0.7 g/L, [ultrasonic] = 60 W, pH= 9.

components and chromophore groups respectively [31,32], which decreased after 120 min, indicating the effective removal on benzene components and chromophore groups of HAs. The molecular weight of size-graded NOM had a good correlation with the spectral slopes radio S_R, which increased with the decrease of the molecular weight of NOM [33]. After calculation, the spectral coefficient S_R increased from 0.85 to 1.30, suggesting the decrease of molecular weight with oxidation of HAs. Fig.3d. demonstrated the difference of the separation state with biochar before and after reaction. It can be clearly observed that after reaction, the color of the solution became lighter due to combined effects such as the adsorption of biochar, the rupture of humic polymers, and the reaction of active species and humic chromophores. The above results indicated that the introduction of ultrasonic treatment accelerated the reaction rate and improved the oxidation efficiency.

The fluorescence spectra of the reaction solution were shown in Fig. 4. From Fig. 4a, four main characteristic fluorescence regions were detected, namely Ex/Em= 200–250/280–380 nm, Ex/Em= 250–450/380–550 nm, Ex/Em= 200–250/380–550 nm, and Ex/Em= 250–450/280–380 nm, which assigned to protein-like small molecules, HAs, fulvic acids and soluble microbial products (SMP) respectively. After 120 min of reaction, the fluorescence intensity decreased significantly in the sole biochar (Fig. 4c) and the combined biochar/persulfate (Fig. 4d) systems. Almost all the characteristic peaks disappeared in the combined biochar/persulfate/ultrasonic system (Fig. 4 h). In comparison, there was a slight change of fluorescence intensity for persulfate (Fig. 4b) and the ultrasonic treatment system (Fig. 4e). The result was consistent with the change of solution UV_{254} of different systems, indicating that the biochar/persulfate/ultrasonic system has a synergistic effect on removal of the above mentioned fluorescent components.

3.3. *Key factors determine performance of the combined system*

To evaluate the effect of biochar dosage on the removal efficiency of HAs, a series of investigations were conducted involving a 120 min ultrasonic-catalytic process with 1 mM persulfate and biochar dosage range of 0.1–0.7 g/L. As shown in Fig. 5a, the removal efficiency of HAs in the combined biochar/persulfate/ultrasonic process increased from 50.0% to 92.4% as the biochar dosage increased from 0.1 g/L to 0.7 g/L due to the increased activated sites and more reactive radicals produced by the synergistic effects between persulfate oxidation, biochar adsorption and ultrasonic irradiation. With the increasing concentration of persulfate, the removal of HAs increased firstly and decreased subsequently (Fig. 5b). The removal of HAs is unfavorable when the concentration of persulfate exceeds a certain range [34,35]. In addition, it has been reported that the number of cavitation bubbles per unit volume in the ultrasonic oxidation system decreases at higher viscosity, which would induce cavitation [36]. Fig. 5c also demonstrated that the removal rate decreased with the increased concentration of HAs.

pH is an essential parameter for the persulfate-AOP processes, determining organics' state and biochar's surface electrical properties [37]. As shown in Fig. 5d, the removal efficiency of HAs did not vary significantly under the experimental conditions, with the removal efficiencies of 93.7%, 91.7%, 90.6%, 88.3% and 91.0% at pH= 5.0, 6.0, 7.0, 8.0 and 9.0, respectively. The value of the point of zero charge (pHzpc) of the biochar measured was 7.0, which would lead to a decrease in the adsorption of HA and PS by biochar at higher pH due to high negative

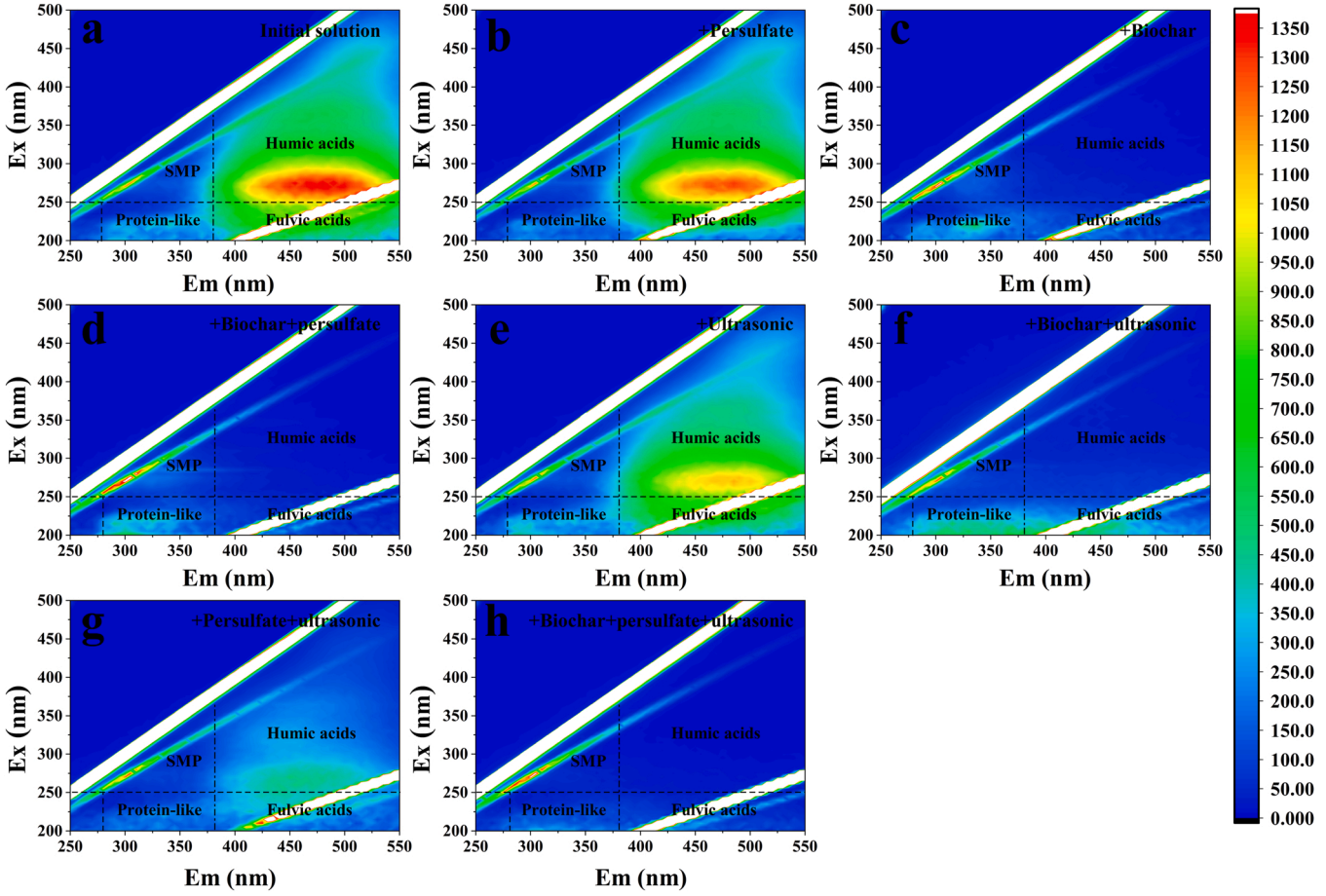

Fig. 4. 3D-EEM spectra of reaction solutions by different processes. (a): original humic acids solution. (b): persulfate alone; (c): biochar alone; (d): biochar/persulfate; (e): ultrasonic alone; (f): biochar/ultrasonic; (g): persulfate /ultrasonic and (h): biochar/persulfate/ultrasonic. Reaction conditions: [humic acids] = 5 mg/L, $[persulfate]_0$ = 1 mM, [biochar] = 0.7 g/L, [ultrasonic] = 60 W, pH= 9.

charge. While under acidic conditions, the surface of biochar was positive. And with the continuous decomposition of persulfate to release H^+ [38], the pH after the reaction was lower than that before the reaction (Table. S2). In this case, the enrichment of humic acid and $S_2O_8^{2-}$ onto the biochar was favored. Although persulfate activation by alkali is not obvious when the initial pH is less than 12.0, ultrasonic might accelerate the alkali activation of persulfate and improve the yield of free radicals at a lower alkaline pH of 9.4 [27]. Considering the subsequent practical water application, pH of 9.0 was used for the next experiments.

3.4. Possible reaction mechanism and the role of ultrasonic promotion

A radical quenching investigation was performed to identify the contribution of different radicals. Tert-butyl-alcohol (TBA) and methanol (MeOH) were selected as the quencher for the •OH and $SO_4^{\bullet-}$ radicals respectively [39–41]. Fig. 6a and b showed the inhibition of TBA or MeOH on the removal of HAs at different molar ratios to persulfate. Compared with the original reaction solution, the removal efficiency decreased from 92.0% to 66.0% (n[TBA/persulfate] =500) and 57.0% (n[TBA/persulfate] =1000) respectively. The slight inhibition of MeOH on the removal efficiency (n[MeOH/persulfate]=1000) implied the minor contribution of $SO_4^{\bullet-}$ to the reaction. The greater affinity of TBA to •OH implied that in the biochar/persulfate/ultrasonic reaction system, •OH was the dominant free radical.

DMPO was used as the spin-trapping agent in the EPR analysis to further confirm the radical species produced in the biochar/persulfate/ultrasonic system. As shown in Fig. 6c, DMPO-X with an intensity ratio of 1:2:1:2:1:2:1 was detected in the biochar/persulfate/ultrasonic treatment system, which is an oxidized derivative produced by the oxidation of DMPO. Some studies have also found such phenomenon in the biochar/ persulfate systems [42–44]. They attributed the production of DMPO-X to the reaction between DPMO and •OH and $SO_4^{\bullet-}$ generated from the activation of persulfate. Combined with the quenching experiment, the results suggested that •OH and $SO_4^{\bullet-}$ were produced in the reaction, and •OH was the dominant radical.

To observe the change of molecular weight of HAs before and after reaction, GPC combined with UV absorbance at 254 nm was applied. Compared with the initial solution of HAs with relatively higher peak area and height at 21.6–28.4 min, the peak retention time was delayed to 22.5–30 min and the peak intensity and area also decreased significantly after treatment (Fig. 6d), suggesting that the HAs were decomposed into smaller molecular weight fragments [45]. This result was consistent with the increase of spectral coefficient S_R after reaction in wavelength detection (Fig. 3c).

Based on the above results, a possible reaction mechanism for the HAs removal by biochar/persulfate/ultrasonic treatment was inferred. Firstly, the adsorption of biochar enriched HAs and persulfate on the surface of biochar. Ultrasonic irradiation would produce a high-temperature environment of up to 5000 K inside bubbles and near the inter-phase of cavitation, so it can remove organic matter effectively [46]. Researchers have proposed that ultrasonic irradiation can alter the DOC composition and lead to disassociation or protonation of carboxylic and phenolic hydroxyl groups of HAs, making it more degradable and less harmful [47,48]. Meanwhile, the extreme physical conditions caused by the collapse of cavitation bubbles produced radicals from decomposition of H_2O and O_2, simultaneously initiating breakage of the

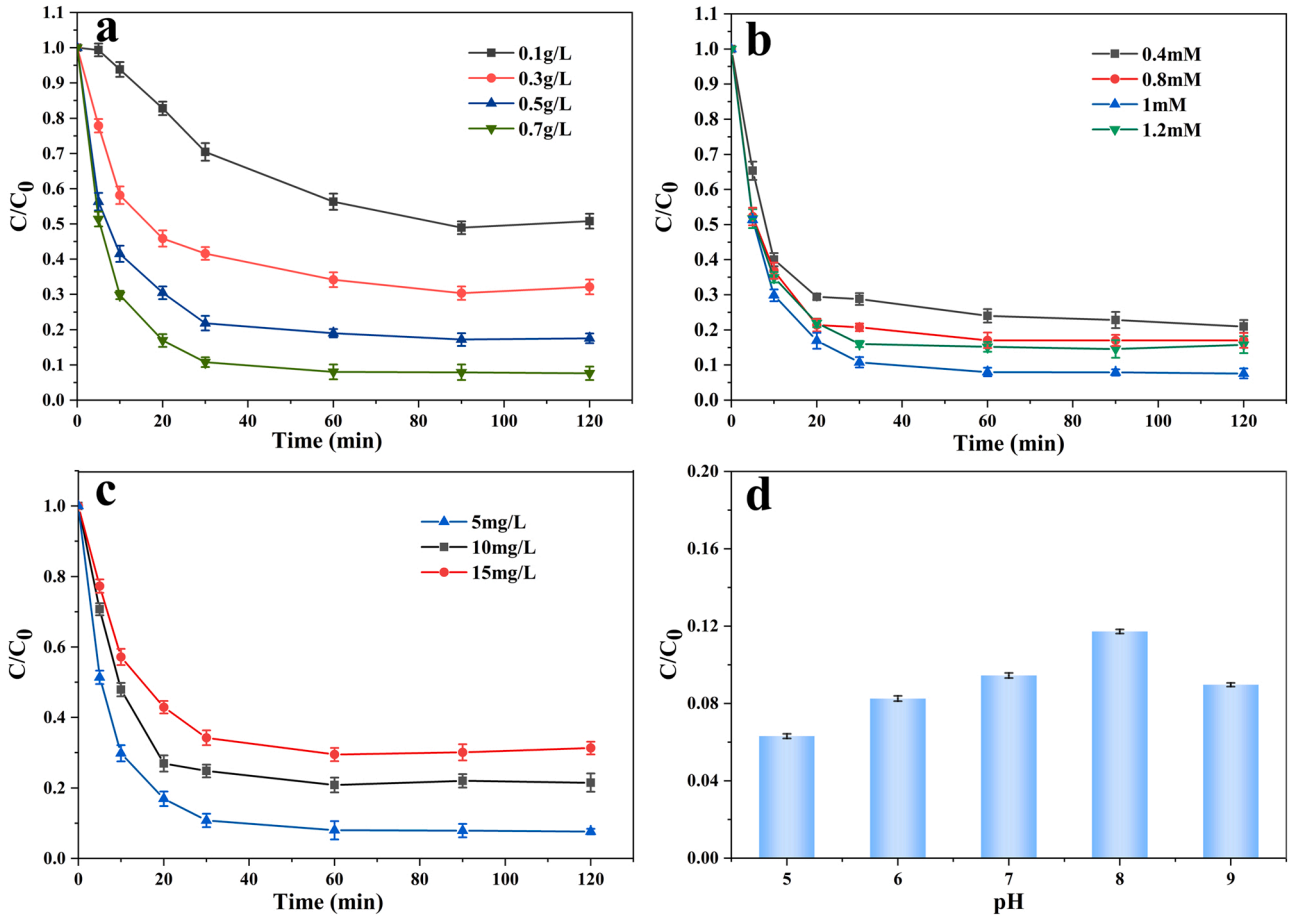

Fig. 5. Effects of various operating parameters on the removal of humic acids, (a) biochar dosages; (b) persulfate dosages; (c) humic acids concentration; (d) pH. Reaction conditions: [biochar] = 0.1–0.7 g/L, $[persulfate]_0$ = 0.2–1.2 mM, [humic acids] = 5–15 mg/L, pH= 5–9, [ultrasonic] = 60 W.

O-O bond in persulfate to generate $SO_4^{\bullet-}$ according to Eqs. (5)–(8) [49,50]. This may also explain why the combined treatment of ultrasonic and persulfate presented better removal efficiency than ultrasonic and persulfate alone. In addition to the oxidation of persulfate, the introduction of ultrasonic can enhance the oxidation of the system (Fig.S1). The oxygen-containing functional groups on the surface of biochar could act as active sites activating persulfate to form free radicals. With the decomposition of persulfate, the pH was reduced and the adsorption of organic matter and persulfate by biochar was further promoted [51]. In this case, HAs could be better removed by oxidation and adsorption of the composite system (Fig. 7).

$$H_2O+))) \rightarrow HO\bullet + \bullet H \quad (5)$$

$$S_2O_8^{2-}+))) \rightarrow 2SO_4^{\bullet-} \quad (6)$$

$$O_2+))) \rightarrow 2\bullet O \quad (7)$$

$$SO_4^{\bullet-}+OH^- \rightarrow SO_4^{2-} + HO\bullet \quad (8)$$

where the symbol "))" denotes ultrasonic irradiation.

Since ultrasonic treatment can clean the surface of biochar, a portion of HAs and small molecular intermediates could be desorbed from the particle surface and re-exposed the active sites to the surface of biochar. Meanwhile ultrasonic irradiation could bring about violent turbulence in the aqueous solution, increasing the reaction and the mass transfer rates by fluidizing the biochar effectively [52]. Generally, •OH, $SO_4^{\bullet-}$ and $^1O_2$ are the primary active species in metal-free carbon materials-persulfate systems [53]. Usually, superoxide ion radical was an intermediate produced by other active species, which was unstable in water [54]. Some scholars found that graphene structure in biochar can catalyze persulfate to produce $^1O_2$, which could also be produced through C = O mediating [55–57]. The removal process may involve not only free radical pathways, but also non-radical pathways such as $^1O_2$, although less possible since $^1O_2$ has low reactivity to natural organic matters, including electron transfer [6,58]. Therefore, the removal of HAs was mostly carried out by adsorption and oxidation with primary radicals such as $SO_4^{\bullet-}$ and •OH, which might also be aided by the non-radical pathway although its role was minor.

3.5. *Application prospects in real water treatment and the reusability of biochar*

This study used the raw water from a reservoir in the Yangtze River to explore practical application prospects of the biochar induced AOP technology. We used three-dimensional fluorescence diagram and fluorescence regional integration (FRI) to analyze the content of organic matters [59]. Figs. 8a and 8b showed the changes of three-dimensional fluorescence spectra of HAs in raw water before and after the persulfate/biochar/ultrasonic treatment. The corresponding characteristic peaks almost disappeared and no new fluorescent substances appeared after 120 min of reaction. As observed in Fig. 8c, FRI values of four organic compounds in water decreased significantly, which was consistent with the characterization of three-dimensional fluorescence. The TOC of the solution after reaction was 0.56 mg/L with the removal rate of 77.7%, indicating that organic compound in the solution were effectively removed and the persulfate/biochar/ultrasonic treatment can be applied to practice effectively. The quality of the actual water used was listed in Table 2.

The biochar was reused for three repeated persulfate/biochar/

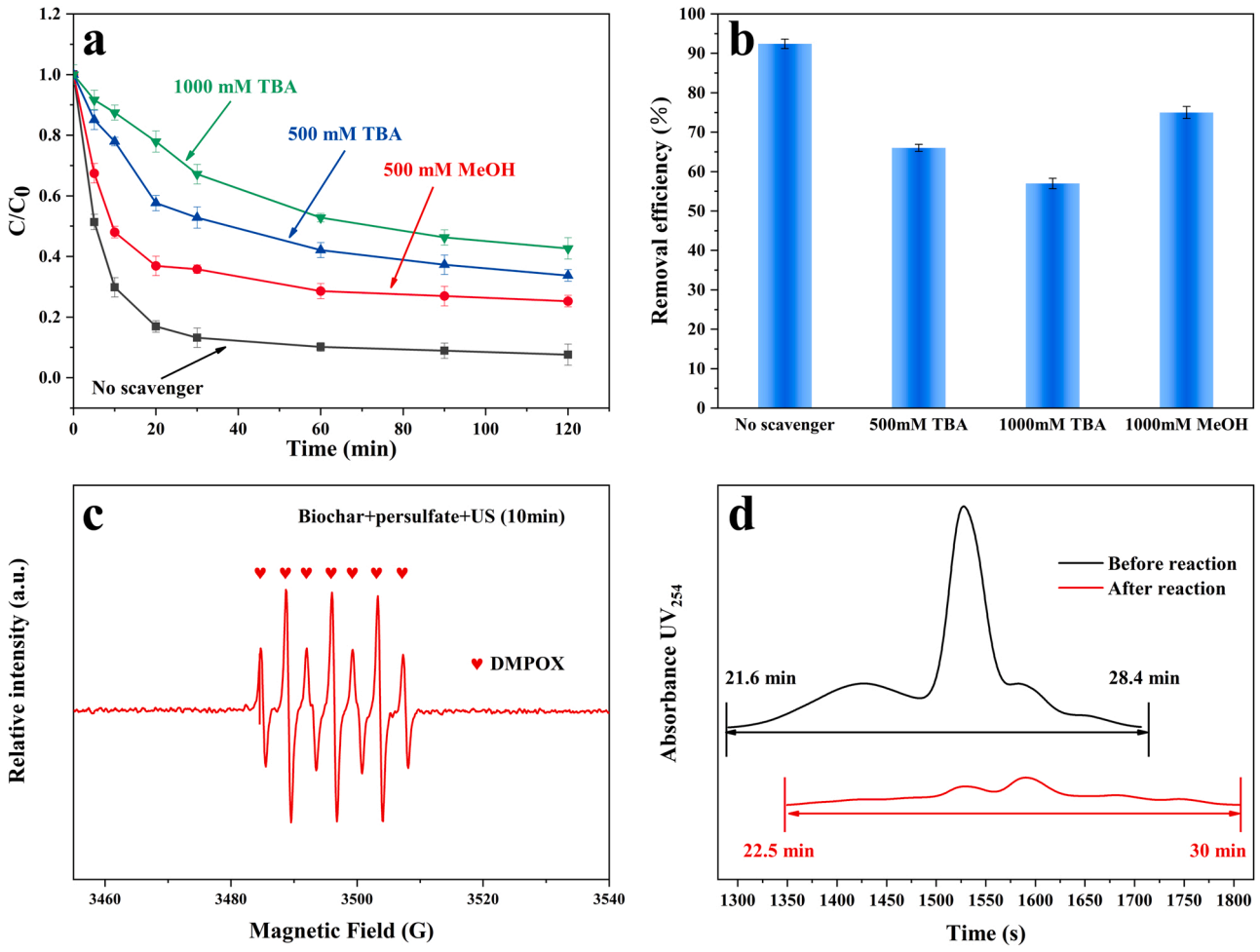

Fig. 6. Radical quenching tests (a) and (b); EPR spectra with DMPO (c) and molecular size distribution chromatograms of humic acids before and after reaction ([biochar] = 0.7 g/L, $[persulfate]_0$ = 1 mM, [humic acids] = 5 mg/L, pH= 9, [ultrasonic] =60 W).

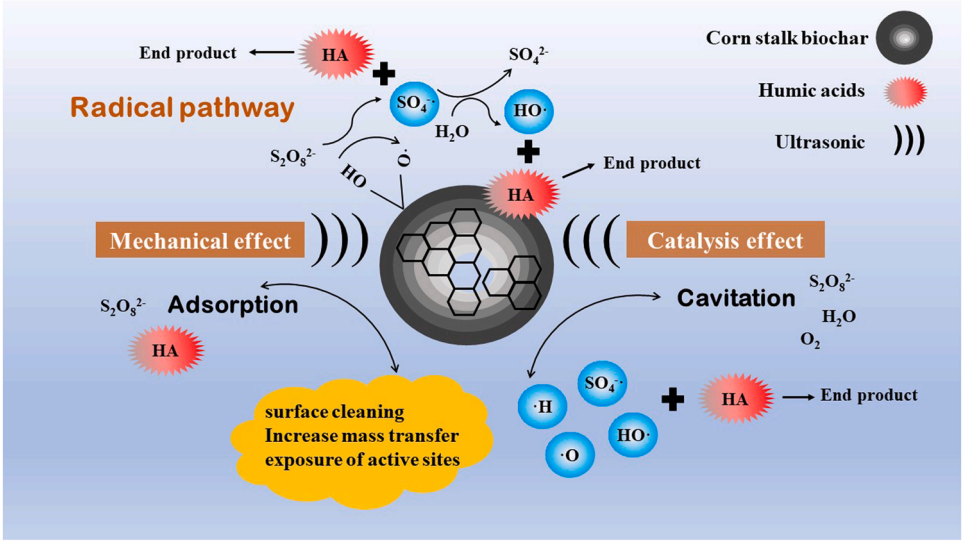

Fig. 7. Mechanism diagram of humic acids removal by ultrasonic enhanced persulfate combined with biochar.

ultrasonic treatment runs to study its re-usability. As shown in Fig. 8d, the virgin biochar could remove more than 90.0% of HAs in 2 h, but only 68.0% and 55.0% of HAs were removed after the second and the third recycles (cycle 2 and 3) respectively. The biochar/persulfate/ultrasonic system presented better recycling capacity of biochar, since the removal efficiency decreased from 87.0% to 39.0% for the second recycle, and 28.0% for the third recycle in our previous combined biochar/persulfate system [15]. The reason may be that when the ultrasonic treatment acts

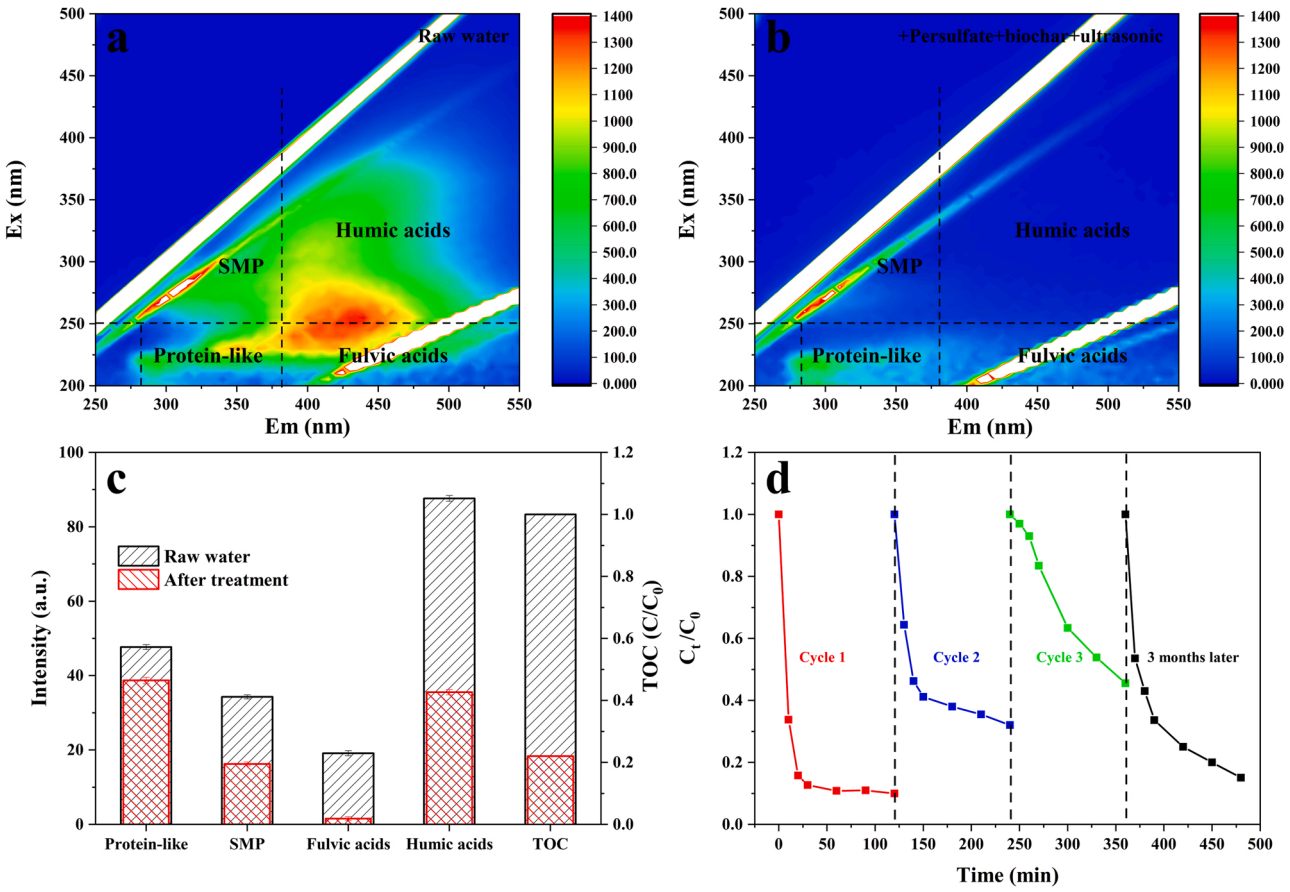

Fig. 8. 3D-EEM before(a) and after(b) reaction;(c) fluorescence intensity of three-dimensional fluorescence components and TOC of raw water before and after reaction;(d) cycle experiments ([biochar] = 0.7 g/L, $[persulfate]_0$ = 1 mM, [humic acids] = 5 mg/L, pH= 9, [ultrasonic] =60 W).

Table 2
Basic parameters of the raw water quality.

Parameters	Average Value
pH	8.6
Conductivity (μS/cm)	341.2
Total organic carbon (TOC) (mg/L)	2.50
Dissolved oxygen (DO) (mg/L)	6.74
Temperature (℃)	29.2

on the liquid, it would produce a large number of cavitation bubbles, which could produce shock waves around, so as to separate the organics adsorbed on the surface of biochar and release active sites [60]. After three months of storage, the biochar could still remove more than 80.0% of HAs. The above results showed that the stability of the biochar was acceptable, but the recycling performance should be improved.

In this study, the main energy input of the experimental device was the ultrasonic cleaner. In order to further compare the energy efficiency of the application system in removing humic acid, the method reported by Bolton et al. can be used to calculate the electric energy per order (EEO, kWh/m^3) [61]. The formula could be simplified to

$$EEO = \frac{38.4P}{Vk} \quad (9)$$

where P = the power of the proposed system [kW], V=the volume of the solution treated (L), k = the first order rate constant (min^{-1}).

Among all systems, the lowest EEO value of 678 kWh/m^3 was obtained for the biochar/persulfate/ultrasonic system, which achieved the highest removal rate for HAs. Azar Fattahi et al. found that the energy required for UV_{254} removal of the system of LED with continuous irradiation of 405 nm, combined with P25 was 539.84 kW h/m^3, which only showed little NOM removal rate [62]. Gora et al. used TiO_2 nanobelts calcined at different temperatures and UVA-LED to degrade DOC in Otonabee River and Ottawa River water, whose maximum required energy reached 1085 kWh/m^3 [63,64]. Since the biochar/persulfate/ultrasonic system could achieve 90% removal rate for HAs within 60 min, the reaction time can be shortened according to the actual situation in order to reduce energy loss.

4. Conclusion

In this study, a synergistic effect on the removal of HAs occurred in the combined biochar/persulfate/ultrasonic treatment process. 90% removal rate for HAs could be reached within 60 min by such combined system with k_{obs} of 3.4×10^{-2} min^{-1}, faster than that of other systems, which showed a synergy index of 2.76. Furthermore, the system showed wide pH adaptability. The adsorption of HAs played an important role in the removal process. •OH and $SO_4^{\bullet-}$ also participated in the oxidation process, where •OH was the main radical. Investigations with actual water showed that this method had good removal effect on removal of macromolecular organic matter and small molecular organic matter from water. The introduction of ultrasonic treatment could improve the reusability of biochar, enhance the oxidation efficiency and improve the reaction rate.

CRediT authorship contribution statement

Hongbo Liu: Funding acquisition, Conceptualization and part of the draft manuscript, Project administration, Supervision. **Mengting Ye**: Lab investigations and part of the draft manuscript, Methodology,

Mechanism modeling. **Zhenxing Ren**: Part of the lab investigations, Methodology. **Eric Lichtfouse**: Writing – review & editing. **Zhongbing Chen**: Writing – review & editing.

Declaration of Competing Interest

The authors declare that they have no known competing financial interests or personal relationships that could have appeared to influence the work reported in this paper.

Acknowledgments

The authors would like to acknowledge the co-funding of this work by the Natural Science Foundation of Shanghai (No. 22ZR1443200) and the National Natural Science Foundation of China (No. 52070130).

Appendix A. Supporting information

Supplementary data associated with this article can be found in the online version at doi:10.1016/j.jece.2022.107809.

References

[1] M. Corona-Bautista, A. Picos-Benítez, D. Villaseñor-Basulto, E. Bandala, J. M. Peralta-Hernández, Discoloration of azo dye Brown HT using different advanced oxidation processes, Chemosphere 267 (2021), 129234, https://doi.org/10.1016/j.chemosphere.2020.129234.

[2] L. Liu, Z. Chen, J. Zhang, D. Shan, Y. Wu, et al., Treatment of industrial dye wastewater and pharmaceutical residue wastewater by advanced oxidation processes and its combination with nanocatalysts: A review, J. Water Process Eng. 42 (2021), 102122, https://doi.org/10.1016/j.jwpe.2021.102122.

[3] D. Ouyang, Y. Chen, J. Yan, L. Qian, L. Han, et al., Activation mechanism of peroxymonosulfate by biochar for catalytic degradation of 1,4-dioxane: Important role of biochar defect structures, Chem. Eng. J. 370 (2019) 614–624, https://doi.org/10.1016/j.cej.2019.03.235.

[4] T. Zhang, Y. Yang, X. Li, H. Yu, N. Wang, et al., Degradation of sulfamethazine by persulfate activated with nanosized zero-valent copper in combination with ultrasonic irradiation, Sep. Purif. Technol. 239 (2020), https://doi.org/10.1016/j.seppur.2020.116537.

[5] J. Faheem, S.H. Du, M.A. Kim, S. Hassan, Irshad, et al., Application of biochar in advanced oxidation processes: supportive, adsorptive, and catalytic role, Environ. Sci. Pollut. Res. 27 (2020) 37286–37312, https://doi.org/10.1007/s11356-020-07612-y.

[6] Y. Zhao, X. Yuan, X. Li, L. Jiang, H. Wang, Burgeoning prospects of biochar and its composite in persulfate-advanced oxidation process, J. Hazard. Mater. 409 (2021), 124893, https://doi.org/10.1016/j.jhazmat.2020.124893.

[7] H. Kan, T. Wang, J. Yu, G. Qu, P. Zhang, et al., Remediation of organophosphorus pesticide polluted soil using persulfate oxidation activated by microwave, J. Hazard. Mater. 401 (2021), 123361, https://doi.org/10.1016/j.jhazmat.2020.123361.

[8] L. Chen, X. Jiang, R. Xie, Y. Zhang, Y. Jin, et al., A novel porous biochar-supported Fe-Mn composite as a persulfate activator for the removal of acid red 88, Sep. Purif. Technol. 250 (2020), 117232, https://doi.org/10.1016/j.seppur.2020.117232.

[9] L. Hu, P. Wang, G. Zhang, G. Liu, Y. Li, et al., Enhanced persulfate oxidation of organic pollutants and removal of total organic carbons using natural magnetite and microwave irradiation, Chem. Eng. J. 383 (2020), https://doi.org/10.1016/j.cej.2019.123140.

[10] K.W. Jung, S.Y. Lee, Y.J. Lee, J.W. Choi, Ultrasound-assisted heterogeneous Fenton-like process for bisphenol A removal at neutral pH using hierarchically structured manganese dioxide/biochar nanocomposites as catalysts, Ultrason Sonochem. 57 (2019) 22–28, https://doi.org/10.1016/j.ultsonch.2019.04.039.

[11] F. Sepyani, R. Darvishi Cheshmeh Soltani, S. Jorfi, H. Godini, M. Safari, Implementation of continuously electro-generated Fe3O4 nanoparticles for activation of persulfate to decompose amoxicillin antibiotic in aquatic media: UV254 and ultrasound intensification, J. Environ. Manag. 224 (2018) 315–326, https://doi.org/10.1016/j.jenvman.2018.07.072.

[12] Y.Q. Gao, N.Y. Gao, W. Wang, S.F. Kang, J.H. Xu, et al., Ultrasound-assisted heterogeneous activation of persulfate by nano zero-valent iron (nZVI) for the propranolol degradation in water, Ultrason Sonochem. 49 (2018) 33–40, https://doi.org/10.1016/j.ultsonch.2018.07.001.

[13] Q. Wang, Y. Cao, H. Zeng, Y. Liang, J. Ma, et al., Ultrasound-enhanced zero-valent copper activation of persulfate for the degradation of bisphenol AF, Chem. Eng. J. 378 (2019), https://doi.org/10.1016/j.cej.2019.122143.

[14] O.S. Arvaniti, F. Bairamis, I. Konstantinou, D. Mantzavinos, Z. Frontistis, Degradation of antihypertensive drug valsartan in water matrices by heat and heat/ultrasound activated persulfate: Kinetics, synergy effect and transformation products, Chem. Eng. J. Adv. 4 (2020), https://doi.org/10.1016/j.ceja.2020.100062.

[15] H. Liu, M. Ye, X. Dong, Z. Ren, S. Long, et al., Removal of humic substances by the synergistic effect of biochar adsorption and activation of persulfate, J. Water Process Eng. 44 (2021), https://doi.org/10.1016/j.jwpe.2021.102428.

[16] S. Wang, N. Zhou, Removal of carbamazepine from aqueous solution using sono-activated persulfate process, Ultrason Sonochem. 29 (2016) 156–162, https://doi.org/10.1016/j.ultsonch.2015.09.008.

[17] R. Conti, A.G. Rombolà, A. Modelli, C. Torri, D. Fabbri, Evaluation of the thermal and environmental stability of switchgrass biochars by Py–GC–MS, J. Anal. Appl. Pyrolysis 110 (2014) 239–247, https://doi.org/10.1016/j.jaap.2014.09.010.

[18] C. Wang, R. Huang, R. Sun, J. Yang, M. Sillanpää, A review on persulfates activation by functional biochar for organic contaminants removal: Synthesis, characterizations, radical determination, and mechanism, J. Environ. Chem. Eng. 9 (2021), https://doi.org/10.1016/j.jece.2021.106267.

[19] X. Zhou, Z. Zeng, G. Zeng, C. Lai, R. Xiao, et al., Persulfate activation by swine bone char-derived hierarchical porous carbon: Multiple mechanism system for organic pollutant degradation in aqueous media, Chem. Eng. J. 383 (2020), https://doi.org/10.1016/j.cej.2019.123091.

[20] C. Guizani, K. Haddad, L. Limousy, M. Jeguirim, New insights on the structural evolution of biomass char upon pyrolysis as revealed by the Raman spectroscopy and elemental analysis, Carbon 119 (2017) 519–521, https://doi.org/10.1016/j.carbon.2017.04.078.

[21] J. Zhang, Q. Wang, Sustainable mechanisms of biochar derived from brewers' spent grain and sewage sludge for ammonia–nitrogen capture, J. Clean. Prod. 112 (2016) 3927–3934, https://doi.org/10.1016/j.jclepro.2015.07.096.

[22] K. Luo, Q. Yang, Y. Pang, D. Wang, X. Li, et al., Unveiling the mechanism of biochar-activated hydrogen peroxide on the degradation of ciprofloxacin, Chem. Eng. J. 374 (2019) 520–530, https://doi.org/10.1016/j.cej.2019.05.204.

[23] B. Shen, Y. Liu, S. Liu, X. Tan, P. Zhang, et al., Catalytic degradation of sulfamethoxazole by persulfate activated with magnetic graphitized biochar: Multiple mechanisms and variables effects, Process Saf. Environ. Prot. 144 (2020) 143–157, https://doi.org/10.1016/j.psep.2020.06.041.

[24] U. Morali, N. Yavuzel, S. Sensoz, Pyrolysis of hornbeam (Carpinus betulus L.) sawdust: Characterization of bio-oil and bio-char, Bioresour. Technol. 221 (2016) 682–685, https://doi.org/10.1016/j.biortech.2016.09.081.

[25] P. Ntzoufra, J. Vakros, Z. Frontistis, S. Tsatsos, G. Kyriakou, et al., Effect of sodium persulfate treatment on the physicochemical properties and catalytic activity of biochar prepared from spent malt rootlets, J. Environ. Chem. Eng. 9 (2021), https://doi.org/10.1016/j.jece.2021.105071.

[26] S. Nikolaou, J. Vakros, E. Diamadopoulos, D. Mantzavinos, Sonochemical degradation of propylparaben in the presence of agro-industrial biochar, J. Environ. Chem. Eng. 8 (2020), https://doi.org/10.1016/j.jece.2020.104010.

[27] Z. Wei, F.A. Villamena, L.K. Weavers, Kinetics and Mechanism of Ultrasonic Activation of Persulfate: An in Situ EPR Spin Trapping Study, Environ. Sci. Technol. 51 (2017) 3410–3417, https://doi.org/10.1021/acs.est.6b05392.

[28] L. Yang, J. Xue, L. He, L. Wu, Y. Ma, et al., Review on ultrasound assisted persulfate degradation of organic contaminants in wastewater: Influences, mechanisms and prospective, Chem. Eng. J. 378 (2019), https://doi.org/10.1016/j.cej.2019.122146.

[29] Y. Wu, J. Guo, Y. Han, J. Zhu, L. Zhou, et al., Insights into the mechanism of persulfate activated by rice straw biochar for the degradation of aniline, Chemosphere 200 (2018) 373–379, https://doi.org/10.1016/j.chemosphere.2018.02.110.

[30] Y. Xue, J. Liu, Y. Zhou, T. Wang, L. Xiang, Treatment of petroleum hydrocarbon contaminated soil by basic oxygen furnace slag activated persulfate oxidation in presence of electromagnetic induction heating, J. Environ. Chem. Eng. 10 (2022), https://doi.org/10.1016/j.jece.2022.107267.

[31] H. Zhang, J. Qu, H. Liu, X. Zhao, Characterization of isolated fractions of dissolved organic matter from sewage treatment plant and the related disinfection by-products formation potential, J. Hazard. Mater. 164 (2009) 1433–1438, https://doi.org/10.1016/j.jhazmat.2008.09.057.

[32] Y. Nie, C. Hu, L. Zhou, J. Qu, Q. Wei, et al., Degradation characteristics of humic acid over iron oxides/Fe0 core–shell nanoparticles with UVA/H2O2, J. Hazard. Mater. 173 (2010) 474–479, https://doi.org/10.1016/j.jhazmat.2009.08.109.

[33] J.R. Helms, A. Stubbins, J.D. Ritchie, E.C. Minor, D.J. Kieber, et al., Absorption spectral slopes and slope ratios as indicators of molecular weight, source, and photobleaching of chromophoric dissolved organic matter, Limnol. Oceanogr. 53 (2008) 955–969.

[34] T. Zhang, Y. Yang, J. Gao, X. Li, H. Yu, et al., Synergistic degradation of chloramphenicol by ultrasound-enhanced nanoscale zero-valent iron/persulfate treatment, Sep. Purif. Technol. 240 (2020), https://doi.org/10.1016/j.seppur.2020.116575.

[35] A. Ziylan-Yavas, Y. Mizukoshi, Y. Maeda, N.H. Ince, Supporting of pristine TiO2 with noble metals to enhance the oxidation and mineralization of paracetamol by sonolysis and sonophotolysis, Appl. Catal. B: Environ. 172- 173 (2015) 7–17, https://doi.org/10.1016/j.apcatb.2015.02.012.

[36] M. Harrabi, H. Belhadj Ammar, K. Mbarki, I. Naifar, C. Yaiche, et al., Ultrasonic power improvement of flumequine degradation effectiveness in aqueous solution via direct and indirect action of mechanical acoustic wave, Ultrason. Sonochem. 48 (2018) 517–522, https://doi.org/10.1016/j.ultsonch.2018.06.004.

[37] X. Du, Y. Zhang, F. Si, C. Yao, M. Du, et al., Persulfate non-radical activation by nano-CuO for efficient removal of chlorinated organic compounds: Reduced graphene oxide-assisted and CuO (0 0 1) facet-dependent, Chem. Eng. J. 356 (2019) 178–189, https://doi.org/10.1016/j.cej.2018.08.216.

[38] Y. Qiu, Q. Zhang, Z. Wang, B. Gao, Z. Fan, et al., Degradation of anthraquinone dye reactive blue 19 using persulfate activated with Fe/Mn modified biochar: Radical/

non-radical mechanisms and fixed-bed reactor study, Sci. Total Environ. 758 (2021), 143584, https://doi.org/10.1016/j.scitotenv.2020.143584.
[39] D. Huang, Q. Zhang, C. Zhang, R. Wang, R. Deng, et al., Mn doped magnetic biochar as persulfate activator for the degradation of tetracycline, Chem. Eng. J. 391 (2020), 123532, https://doi.org/10.1016/j.cej.2019.123532.
[40] Q. Liu, X. Bai, X. Su, B. Huang, B. Wang, et al., The promotion effect of biochar on electrochemical degradation of nitrobenzene, J. Clean. Prod. 244 (2020), 118890, https://doi.org/10.1016/j.jclepro.2019.118890.
[41] S. Liu, C. Lai, B. Li, C. Zhang, M. Zhang, et al., Role of radical and non-radical pathway in activating persulfate for degradation of p-nitrophenol by sulfur-doped ordered mesoporous carbon, Chem. Eng. J. 384 (2020), 123304, https://doi.org/10.1016/j.cej.2019.123304.
[42] X. Rong, M. Xie, L. Kong, V. Natarajan, L. Ma, et al., The magnetic biochar derived from banana peels as a persulfate activator for organic contaminants degradation, Chem. Eng. J. 372 (2019) 294–303, https://doi.org/10.1016/j.cej.2019.04.135.
[43] W. Xiang, Q. Ji, C. Xu, Y. Guo, Y. Liu, et al., Accelerated photocatalytic degradation of iohexol over Co3O4/g-C3N4/Bi2O2CO3 of p-n/n-n dual heterojunction under simulated sunlight by persulfate, Appl. Catal. B: Environ. 285 (2021), https://doi.org/10.1016/j.apcatb.2020.119847.
[44] X. Liu, F. Huang, Y. Yu, P. Zhao, Y. Zhou, et al., Ofloxacin degradation over Cu–Ce tyre carbon catalysts by the microwave assisted persulfate process, Appl. Catal. B: Environ. 253 (2019) 149–159, https://doi.org/10.1016/j.apcatb.2019.04.047.
[45] T. Li, Y. Jiang, X. An, H. Liu, C. Hu, et al., Transformation of humic acid and halogenated byproduct formation in UV-chlorine processes, Water Res. 102 (2016) 421–427, https://doi.org/10.1016/j.watres.2016.06.051.
[46] N.E. Chadi, S. Merouani, O. Hamdaoui, M. Bouhelassa, New aspect of the effect of liquid temperature on sonochemical degradation of nonvolatile organic pollutants in aqueous media, Sep. Purif. Technol. 200 (2018) 68–74, https://doi.org/10.1016/j.seppur.2018.01.047.
[47] R.A. Al-Juboori, L.A. Bowtell, T. Yusaf, V. Aravinthan, Insights into the scalability of magnetostrictive ultrasound technology for water treatment applications, Ultrason. Sonochem. 28 (2016) 357–366, https://doi.org/10.1016/j.ultsonch.2015.08.013.
[48] V. Naddeo, V. Belgiorno, R.M.A. Napoli, Behaviour of natural organic mater during ultrasonic irradiation, Desalination 210 (2007) 175–182, https://doi.org/10.1016/j.desal.2006.05.042.
[49] K. Fedorov, M. Plata-Gryl, J.A. Khan, G. Boczkaj, Ultrasound-assisted heterogeneous activation of persulfate and peroxymonosulfate by asphaltenes for the degradation of BTEX in water, J. Hazard. Mater. 397 (2020), 122804, https://doi.org/10.1016/j.jhazmat.2020.122804.
[50] C.H. Weng, K.L. Tsai, Ultrasound and heat enhanced persulfate oxidation activated with Fe(0) aggregate for the decolorization of C.I. Direct Red 23, Ultrason. Sonochem. 29 (2016) 11–18, https://doi.org/10.1016/j.ultsonch.2015.08.012.
[51] T. Guo, L. Jiang, K. Wang, Y. Li, H. Huang, et al., Efficient persulfate activation by hematite nanocrystals for degradation of organic pollutants under visible light irradiation: Facet-dependent catalytic performance and degradation mechanism, Appl. Catal. B: Environ. 286 (2021), https://doi.org/10.1016/j.apcatb.2021.119883.
[52] C.-H. Weng, K.-L. Tsai, Ultrasound and heat enhanced persulfate oxidation activated with Fe0 aggregate for the decolorization of C.I. Direct Red 23, Ultrason. Sonochem. 29 (2016) 11–18, https://doi.org/10.1016/j.ultsonch.2015.08.012.
[53] J. Yu, H. Feng, L. Tang, Y. Pang, G. Zeng, et al., Metal-free carbon materials for persulfate-based advanced oxidation process: Microstructure, property and tailoring, Prog. Mater. Sci. 111 (2020), https://doi.org/10.1016/j.pmatsci.2020.100654.
[54] T. Guo, L. Jiang, H. Huang, Y. Li, X. Wu, et al., Enhanced degradation of tetracycline in water over Cu-doped hematite nanoplates by peroxymonosulfate activation under visible light irradiation, J. Hazard Mater. 416 (2021), 125838, https://doi.org/10.1016/j.jhazmat.2021.125838.
[55] X. Cheng, H. Guo, Y. Zhang, X. Wu, Y. Liu, Non-photochemical production of singlet oxygen via activation of persulfate by carbon nanotubes, Water Res. 113 (2017) 80–88, https://doi.org/10.1016/j.watres.2017.02.016.
[56] R. Yin, W. Guo, H. Wang, J. Du, Q. Wu, et al., Singlet oxygen-dominated peroxydisulfate activation by sludge-derived biochar for sulfamethoxazole degradation through a nonradical oxidation pathway: Performance and mechanism, Chem. Eng. J. 357 (2019) 589–599, https://doi.org/10.1016/j.cej.2018.09.184.
[57] H. Huang, T. Guo, K. Wang, Y. Li, G. Zhang, Efficient activation of persulfate by a magnetic recyclable rape straw biochar catalyst for the degradation of tetracycline hydrochloride in water, Sci. Total Environ. 758 (2021), 143957, https://doi.org/10.1016/j.scitotenv.2020.143957.
[58] C. Zhao, B. Shao, M. Yan, Z. Liu, Q. Liang, et al., Activation of peroxymonosulfate by biochar-based catalysts and applications in the degradation of organic contaminants: A review, Chem. Eng. J. 416 (2021), https://doi.org/10.1016/j.cej.2021.128829.
[59] J. Chen, E.J. LeBoeuf, S. Dai, B. Gu, Fluorescence spectroscopic studies of natural organic matter fractions, Chemosphere 50 (2003) 639–647, https://doi.org/10.1016/S0045-6535(02)00616-1.
[60] P. Wang, W. Ji, M. Li, G. Zhang, J. Wang, Bi25VO40 microcube with step surface for visible light photocatalytic reduction of Cr(VI): Enhanced activity and ultrasound assisted regeneration, Ultrason. Sonochem. 38 (2017) 289–297, https://doi.org/10.1016/j.ultsonch.2017.03.016.
[61] O.S. Arvaniti, I. Konstantinou, D. Mantzavinos, Z. Frontistis, Destruction of valsartan using electrochemical and electrochemical/persulfate process. Kinetics, identification of degradation pathway and application in aqueous matrices, J. Environ. Chem. Eng. 9 (2021), https://doi.org/10.1016/j.jece.2021.106265.
[62] A. Fattahi, M.J. Arlos, L.M. Bragg, R. Liang, N. Zhou, et al., Degradation of natural organic matter using Ag-P25 photocatalyst under continuous and periodic irradiation of 405 and 365 nm UV-LEDs, J. Environ. Chem. Eng. 9 (2021), https://doi.org/10.1016/j.jece.2020.104844.
[63] S.L. Gora, R. Liang, Y.N. Zhou, S.A. Andrews, Photocatalysis with easily recoverable linear engineered TiO2 nanomaterials to prevent the formation of disinfection byproducts in drinking water, J. Environ. Chem. Eng. 6 (2018) 197–207, https://doi.org/10.1016/j.jece.2017.11.068.
[64] S. Gora, R. Liang, Y.N. Zhou, S. Andrews, Settleable engineered titanium dioxide nanomaterials for the removal of natural organic matter from drinking water, Chem. Eng. J. 334 (2018) 638–649, https://doi.org/10.1016/j.cej.2017.10.058.

Supporting Information

Towards synergistic combination of biochar/ultrasonic persulfate enhancing removal of natural humic acids from water

Hongbo Liu[1*a], Mengting Ye[a], Zhenxing Ren[a], Eric Lichtfouse[b], Zhongbing Chen[c]

a School of Environment and Architecture, University of Shanghai for Science and Technology, 516 Jungong Road, 200093, Shanghai, China. b Aix-Marseille Univ, CNRS, IRD, INRA, Coll France, CEREGE, 13100 Aix en Provence, France. c Faculty of Environmental Sciences, Czech University of Life Sciences Prague, Kamýcká 129, 16500 Prague, Czech Republic

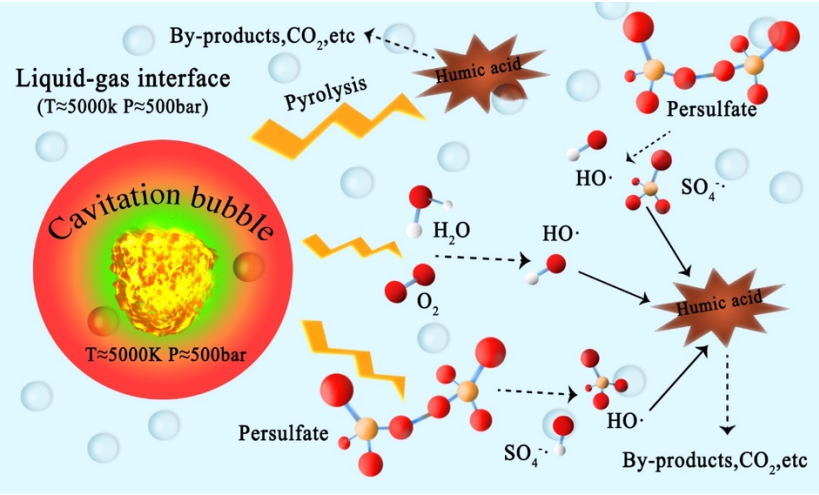

Fig. S1 Synergistic removal of humic acid from water by ultrasonic and persulfate treatments

Table S1 pH changes in different processes

Systems	Initial pH	Final pH
Ultrasonic	9.1	8.7
Persulfate	9.1	8.5
Biochar	9.1	8.4
Biochar +persulfate	9.1	3.1
Ultrasonic +persulfate	9.1	8.7
Biochar +ultrasonic	9.1	8.7
Biochar +persulfate +ultrasonic	9.1	3.1

Table S2 The solution pH values before and after reaction

Initial pH	5	6	7	8	9
Final pH	2.9	3.0	3.0	3.1	3.1

1* Corresponding author ADD: 516, Jungong Road, 200093, Shanghai, China;

Email: Liuhb@usst.edu.cn (H., Liu) Tel: +86(21)55275979; Fax: +86(21)55275979